Disorder effects in Nd^{3+}-doped strontium hexa-aluminate laser crystals

2006 J. Phys.: Condens. Matter 18 597

(http://iopscience.iop.org/0953-8984/18/2/017)

INSTITUTE OF PHYSICS PUBLISHING JOURNAL OF PHYSICS: CONDENSED MATTER

J. Phys.: Condens. Matter **18** (2006) 597–611 doi:10.1088/0953-8984/18/2/017

Disorder effects in Nd^{3+}-doped strontium hexa-aluminate laser crystals

A Lupei[1], V Lupei[1], C Gheorghe[1], L Gheorghe[1], D Vivien[2], G Aka[2] and E Antic-Fidancev[2]

[1] Institute of Atomic Physics, INFLPR-Bucharest, MG 077125, Romania
[2] Laboratoire Chimie Appliquée de L'état Solide, ENSCP, 11 rue Pierre et Marie Curie, 75231 Paris Cedex 05, France

Received 27 September 2005, in final form 16 November 2005
Published 14 December 2005
Online at stacks.iop.org/JPhysCM/18/597

Abstract

The high resolution and polarized absorption spectroscopic data of Nd^{3+}-doped, Mg^{2+}-compensated strontium hexa-aluminate $Sr_{1-x}Nd_yLa_{x-y}Mg_xAl_{12-x}O_{19}$ (ASL: Nd) crystals in an extended compositional range ($0.01 \leqslant x \leqslant 0.5$) are presented. This crystal offers for the Nd^{3+} ions a unique crystallographic site (2d) with 12 O^{2-} coordination and ideal D_{3h} symmetry. The optical spectra in all this compositional range contain contributions from two families of structural centres, C_1 and C_2 (with two components C_2' and C_2''), whose spectral features are mainly dependent on the composition parameter x. The presence of these centres is attributed to the cationic disorder. It is inferred that while the centres C_1 and C_2 are connected with the presence or absence of trivalent ions in the nearest (2d) coordination sphere normally occupied by Sr^{2+}, the two components C_2' and C_2'' are associated to the existence or lack of Mg^{2+} ions in the nearest sphere of Al^{3+} tetrahedral (Al^{3+}_{tetr}) sites. This structural disorder leads to crystal-field perturbations by electric charge difference, although for C_1 centres the perturbation by ionic size differences is also evident. The polarized spectroscopy indicates departures from the selection rules for D_{3h} symmetry for C_1 centres, whereas both polarized spectra and crystal-field analysis confirm the near-D_{3h} symmetry for C_2 centres. The composition dependence of the spectra indicates that the distribution of the La^{3+} and Nd^{3+} ions at the (2d) sites is random, while that of the Mg^{2+} in the Al^{3+}_{tetr} sites is correlated with the former. The connection of this structural model with the EPR data and with earlier models is discussed.

1. Introduction

Owing to the attractive properties, such as the ability to incorporate large concentrations of rare-earth or transition-metal ions and to grow high-quality crystals, strontium hexa-aluminate $SrAl_{12}O_{19}$ is being actively investigated as potential luminescent phosphor or laser material.

The strontium hexa-aluminate crystal has hexagonal magnetoplumbite structure [1] with space group $P6_3/mmc$, is uniaxial with the c-axis perpendicular to the mirror ($\boldsymbol{a}$, $\boldsymbol{b}$ at 120°) plane. The crystallographic unit cell contains two formula units and the Sr^{2+} ions occupy the (2d) sites with 12 O^{2-} coordination and D_{3h} symmetry, placed in the mirror planes that separate two spinel-like groups, while Al^{3+} ions occupy several small sites with tetrahedral, octahedral and fivefold bipyramidal O^{2-} coordination. The Nd^{3+} ions replace part of Sr^{2+} ions in the large cationic (2d) sites, and charge compensation can be accomplished by a partial substitution of Al^{3+} with divalent ions such as Mg^{2+} [2–5], which show preference for the tetrahedral sites [6, 7]. The crystal growth experiments of Nd-doped Mg-compensated strontium aluminate $Sr_{1-x}Nd_xMg_xAl_{12-x}O_{19}$ (in what follows we shall use the abbreviation ASN [3]) have shown that large amounts of Nd^{3+} ions (over 20% with respect to the (2d) sites) enable congruent melting. Although the density of sites available to Nd^{3+} is quite low ($\sim 0.34 \times 10^{22}$ cm^{-3}), such large Nd^{3+} concentrations could produce concentration quenching of emission, that can be prevented by co-doping the crystals with optically inert La^{3+} ions [8–10], resulting in ASL: Nd—$Sr_{1-x}Nd_yLa_{x-y}Mg_xAl_{12-x}O_{19}$ crystals with $0 \leqslant x < 1$ and $y \leqslant x$.

The 12-fold O^{2-} coordination of the (2d) sites determines low covalence for the metal–ligand bonds and low nephelauxetic effects [11, 12] for the doping rare-earth ions as well as moderate crystal-field effects. This makes the strontium aluminate attractive as a host for short-wavelength quasi-three-level $^4F_{3/2} \rightarrow {}^4I_{9/2}$ laser emission of Nd^{3+}. Indeed, laser studies [13] on ASL: Nd have evidenced efficient emission at ~900 nm, one of the shortest wavelengths for this range, with a 58% slope efficiency. A major application of this laser is opened by the generation, by frequency doubling, of blue laser emission, required by various applications such as display or medicine.

The initial x-ray diffraction, optical spectroscopy and EPR data on Nd^{3+} in (Ln, Mg) strontium hexa-aluminates, ASN ($Ln^{3+} = Nd^{3+}$) [3–5] and ASL ($Ln^{3+} = Nd^{3+}$ and La^{3+}) [8–10], as well as the laser emission characteristics [13], have been interpreted in terms of a one-centre model, consisting of a substitutional Nd^{3+} that occupies a (2d) site that preserves the D_{3h} symmetry, although the x-ray investigations have suggested [4] that for large x some Ln^{3+} ions could also occupy sites of lower symmetry (probably C_{2v}) and extra lines have been observed in the optical spectra [4, 5].

Recent high-resolution optical spectroscopy [14–16] of ASL: Nd for $0.2 \leqslant x \leqslant 0.4$, $0.05 \leqslant y \leqslant 0.15$ clearly revealed the presence of two types of structural centre, labelled C_1 and C_2, whose proportion and spectroscopic properties (the line positions, shapes and widths) are determined especially by the composition parameter x. The existence of two structural centres could influence the laser emission properties of ASL: Nd, leading to instabilities or wavelength shifts of laser emission. Indeed, by selection of the optimal compositions of the crystals (with dominance of a unique type of centre) and pumping conditions, improved laser emission characteristics at ~901 nm (slope efficiency 74%) in ASL: Nd have recently been obtained [17].

From the composition dependence of the spectral data it was inferred [14–16] that the two Nd^{3+} centres in ASL have the same basic structure, a Nd^{3+} ion in a (2d) site, with only bivalent Sr^{2+} ions in the nearby (2d) cationic sites for C_2 centres and with one to six trivalent Ln^{3+} (Nd^{3+} or La^{3+}) ions for the C_1 class of centre. However, several basic problems of the spectroscopic and structural properties of this system remain unsolved:

(i) the validity of the composition dependence on x of the two centres at very low and at high x values;

(ii) the difference between the perturbing effect of the La^{3+} and Nd^{3+} ions in nearby (2d) sites on the spectroscopic properties of C_1 centres;

(iii) the perturbing effect of the Mg^{2+} ions (and their distribution in nearby Al^{3+} sites) on the spectroscopic properties of the C_1 and C_2 centres;
(iv) the effect of the cationic disorder on the local symmetry of the centres.

The present paper attempts to answer these problems in a consistent way. The spectral data on crystals with an extended composition range $x = 0.01$–0.5 are analysed in section 3.1. The polarized absorption data for the two centres are examined in terms of the ideal D_{3h} local group (section 3.2). In section 3.3, improved models for non-equivalent centres are proposed and the previous interpretations of the optical or EPR spectra are examined. A crystal-field parametric calculation for the C_2 centre energy levels is performed in section 3.4. In section 3.5 the implication of the presence of two types of structural centres on the laser emission properties of these crystals is briefly analysed.

2. Experiment

Crystals of $Sr_{1-x}Nd_xMg_xAl_{12-x}O_{19}$ (ASN) with $x = 0.01$ and 0.05 and of $Sr_{1-x}Nd_yLa_{x-y}Mg_xAl_{12-x}O_{19}$ (ASL: Nd) with $x = 0.1$–0.5, $y = 0.05$ were grown by Czochralski method in iridium crucibles. For low x (<0.2) the melt is incongruent [10] and the crystal growth is difficult; however, small pieces of crystals with magnetoplumbite structure were obtained.

The absorption spectra at 15 and 300 K were measured with a set-up consisting of a tungsten halogen lamp, a GDM 1 m monochromator with a resolution of $\sim 0.3\ cm^{-1}$, a photon-counting photomultiplier, a Turbo-MCS multichannel analyser and a helium closed-cycle system for low temperatures. The emission spectra at selective excitation were obtained with a CW Ti:sapphire laser (Coherent 890) pumped with an argon-ion laser. The spectra were analysed with an ARC Spectra Pro-7510 monochromator and detected with a cooled InGaAs photodiode.

3. Results and discussion

3.1. Composition dependence of the Nd^{3+} spectra in strontium aluminates

The optical spectroscopic measurements over an extended spectral range (up to $\sim 24\,000\ cm^{-1}$) on Nd^{3+} in ASN and ASL crystals in the enlarged compositional range $0.01 \leqslant x \leqslant 0.5$ confirm the division of the Nd^{3+} centres in two main classes, named previously [15] C_1 and C_2, and reveal new composition-dependent spectral features, that manifest selectively in various transitions.

The most pronounced difference between the two Nd^{3+} structural centres is revealed in the $^4I_{9/2} \rightarrow {}^4F_{3/2}$ spectra, as illustrated in figure 1(a). The spectra evidence the predominance of C_2 centres at low x ($x < 0.05$), and the strong growth of the C_1 centre intensity with x: at $x = 0.5$ its relative intensity is larger than 95%. The effective crystal-field splitting of the $^4F_{3/2}$ manifold, estimated from the peaks in the low-temperature absorption bands, depends on the composition parameters x for both centres (table 1), being about twice as large for the C_1 centre than for C_2, but with similar barycentres (within $\sim$2–3 cm^{-1}). The Nd^{3+} lines in ASL are inhomogeneously broadened: many lines show asymmetric shape, whereas other lines are Gaussian. The full width at half maximum of $^4I_{9/2}(Z_1) \rightarrow {}^4F_{3/2}(R_1)$ lines is centre and composition dependent; for the C_1 centre it increases from $\sim 12\ cm^{-1}$ for $x = 0.05$ to $\sim 25\ cm^{-1}$ for $x = 0.5$, while for the C_2 centre the maximum widths are of $\sim 6\ cm^{-1}$. Due to the smaller widths of the C_2 lines, the peak absorption cross-sections of C_2 lines are much stronger than those of C_1, a misleading fact in the previous interpretations

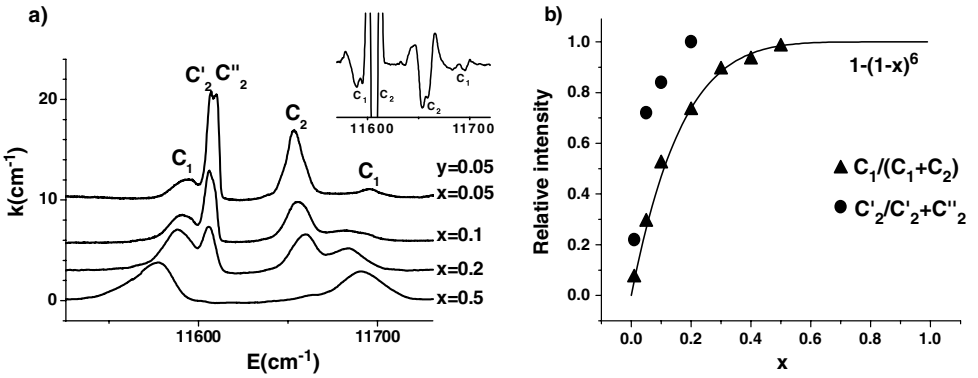

Figure 1. (a) The composition dependence of the $^4I_{9/2} \rightarrow {}^4F_{3/2}$ Nd^{3+} absorption at 15 K of several (Ln, Mg) strontium hexa-aluminates ($x = 0.05$–0.5, $y = 0.05$), measured with unpolarized light along *c*. Inset, the second derivative of the $^4I_{9/2} \rightarrow {}^4F_{3/2}$ absorption for ASL: Nd ($x = 0.1$, $y = 0.05$ sample). (b) The composition (x) dependence of the relative intensity of C_1 and C_2 centres (triangles) and C_2' and C_2'' (circles) measured from Nd^{3+} $^4I_{9/2}(Z_1) \rightarrow {}^4F_{3/2}(R_1)$ absorption at 15 K. The solid line is the theoretical curve $(1 - (1 - x)^6)$.

Table 1. Low-temperature (15 K) effective crystal-field splitting of Nd^{3+} $^4F_{3/2}$ manifold for C_1 and C_2 centres in (Ln, Mg) strontium aluminate crystals with different x parameters.

	Effective crystal-field splitting of the $^4F_{3/2}$ (in cm^{-1}) Structural centre	
Composition parameter, x	C_1	C_2
0.01	—	$C_2' \sim 48$ $C_2'' \sim 40$
0.05	C_1 (Nd) ∼100	$C_2' \sim 48$ $C_2'' \sim 40$
0.1	C_1 (Nd) ∼100 C_1 (La) ∼94	$C_2' \sim 53$ $C_2'' \sim 44$
0.2	97	54.5
0.3	100.8	58.1
0.4	106.8	59.3
0.5	111	60.2

of the spectra. The peaks of the C_1 and C_2 lines are almost coincident in the $^4I_{9/2} \rightarrow {}^2P_{1/2}$ absorption at 15 K, and a single line was observed for $0.2 \leqslant x \leqslant 0.4$, leading to a single centre model [4, 5, 9]. However, the high-resolution measurements [15] for the same compositional range revealed that this line is asymmetric and its shape and width depend on composition. The present measurements show that at very low x (< 0.1) this line has two components (with a splitting of ∼4 cm^{-1}), whose relative intensities parallel the data in the $^4I_{9/2} \rightarrow {}^4F_{3/2}$ absorption.

In many high-resolution absorption spectra at 15 K, due to the reduced linewidths at low x ($\leqslant 0.05$), C_2 centre lines show a clear splitting into two components C_2' and C_2'', as illustrated in figure 1(a) for the $^4I_{9/2}(Z_1) \rightarrow {}^4F_{3/2}(R_1)$ transition. The shift between the C_2' and C_2'' components is ∼4–5 cm^{-1} and the intensity of the C_2' line increases strongly with x and at $x = 0.05$ it becomes practically equal to that of C_2'' (figure 1(a)). Over $x = 0.2$

the C_2' component is dominant and accounts for the previously analysed C_2 centre [15]. The two components are almost Gaussian: the C_2'' line is very sharp, ∼1–2 cm^{-1}, while the C_2' component is broader, ∼4–5 cm^{-1}, and its linewidth increases with x. For small x ($\leqslant 0.1$) table 1 gives the crystal-field splittings of $^4F_{3/2}$ for both components C_2'' and C_2', while for larger x it presents those of $C_2 \equiv C_2'$.

The relative global intensity of the C_1 centre for the new compositions investigated here, estimated from the ratio of the area of the low-temperature $^4I_{9/2}(Z_1) \rightarrow {}^4F_{3/2}(R_1)$ absorption line to the sum of areas of C_1 and C_2 lines (triangles in figure 1(b)), confirms an increase with the parameter x according to the $1-(1-x)^6$ law (continuous line in figure 1(b)) [15]; see later in section 3.3. The relative intensity of the C_2' centre with respect to the global intensity of the C_2' and C_2'' centres (circles in figure 1(b)) grows much stronger with x.

In our previous investigations [15] only the global effects associated to the perturbations induced by Ln^{3+} ions in nearby (2d) sites were observed. In order to detect *ionic size effects* of nearby Nd^{3+} or La^{3+} ions, the 15 K absorption spectra of $Sr_{1-x}Nd_yLa_{x-y}Mg_xAl_{12-x}O_{19}$ with different x, y parameters were compared. Thus, while for the crystal without La^{3+} ($x = y = 0.05$) each of the two transitions, $^4I_{9/2}(Z_1) \rightarrow {}^4F_{3/2}(R_1)$ and $^4I_{9/2}(Z_1) \rightarrow {}^4F_{3/2}(R_2)$, of the C_1 centre consist of a single line, in the crystal with 0.05 La and 0.05 Nd ($x = 0.1$, $y = 0.05$), these transitions are composed of two lines of about the same intensity (see the second derivative of absorption for $x = 0.1$, $y = 0.05$ sample, inset in figure 1(a)). Obviously, these two components of the C_1 lines correspond to the centres for which the perturbing effect is determined by Nd^{3+} (C_1 (Nd)-centre) and respectively La^{3+} (C_1 (La)-centre) ions in the nearest (2d) coordination sphere. The crystal-field splitting for C_1 (Nd) is larger than for C_1 (La) (table 1) and the barycentre of the $^4F_{3/2}$ manifold is slightly higher. By keeping the parameter y constant and increasing x, the intensity of last line becomes dominant (figure 1). Such size effects were not remarked in the $^4I_{9/2} \rightarrow {}^4F_{3/2}$ absorption spectra of C_2 centres.

The laser excited emissions of the C_1 and C_2 centres depend on the parameter x and show systematic shifts by tuning the excitation inside the absorption lines, especially for the C_1 centre. This confirms that the inhomogeneously broadened lines are envelopes of lines corresponding to slightly different structural centres. Figure 2 presents the 15 K $^4F_{3/2} \rightarrow {}^4I_{9/2,11/2,13/2}$ emission spectra under excitation at the peak of the absorption lines for two crystals where one or the other centre prevails ($x = 0.05$ for C_2 and $x = 0.5$ for C_1). The excitation was done in $^4F_{3/2}$ (transition $Z_1 \rightarrow R_2$ for C_1 and $Z_1 \rightarrow R_1$ for C_2) along the c axis; L denotes the laser excitation wavelengths. It is obvious that the emission spectra for these centres are different. Effective Stark level energies (inferred from the line peaks) for the $^4F_{3/2}$ and $^4I_{9/2}$ manifolds involved in the 900 nm laser emission of the C_1 centre in the crystal with $x = 0.5$ and those for C_2 in case of $x = 0.05$ are given in table 2. In table 2 the irreducible representations (IRs) of D_{3h} group associated to Stark levels of C_2 centre are also given (see section 3.2). Based on the differences observed in table 2, it is obvious that one cannot speak of an energy-level scheme for Nd^{3+} in ASN or ASL in the model of a single centre.

While for the C_1 centre one could speak only of the *effective energy levels* at a given composition, the positions of the spectral lines for the $C_2 \equiv C_2'$ Nd^{3+} centre for $x \leqslant 0.2$ do not change significantly with x (figure 1). Therefore, an actual experimental energy-level scheme could be tentatively assigned for the C_2 Nd^{3+} centre in ASN from 15 to 300 K absorption or low-temperature selectively excited emission for the $x = 0.05$ sample. Whereas in the $^4I_J \Leftrightarrow {}^4F_{3/2}$ transitions the lines belonging to the two centres could be clearly separated, in other ranges, especially at high energies, this identification is more difficult. Part of the experimentally determined energy levels at 15 K are given in table 3. The experimental Stark levels in parentheses refer to weak lines in the spectra and they could be attributed to the C_1

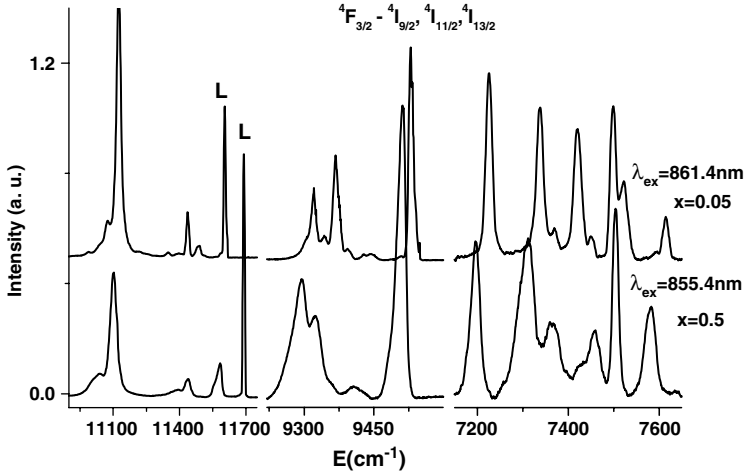

Figure 2. The 15 K Nd^{3+} $^4F_{3/2} \rightarrow {}^4I_{9/2,11/2,13/2}$ emission spectra under selective excitation in the absorption peaks of the two centres (for C_2 at 861.4 nm in a sample with $x = y = 0.05$ and for C_1 at 855.4 nm in a sample with $x = 0.5$, $y = 0.05$; L are the laser excitation lines).

Table 2. The Stark levels of the Nd^{3+} $^4I_{9/2}$ and $^4F_{3/2}$ manifolds for the $C_2 \equiv C_2'$ centre (in the crystal with $x = y = 0.05$) and for the C_1 centre (in crystals with $x = 0.5$, $y = 0.05$).

Manifold	Stark levels	C_2 ($x = 0.05$)	C_2[a] IR in D_{3h}	C_1 ($x = 0.5$)
	Z_1	0	Γ_8	0
	Z_2	110	Γ_7	140
$^4I_{9/2}$	Z_3	155	Γ_9	175
	Z_4	480	Γ_9	480
	Z_5	530	Γ_8	545
$^4F_{3/2}$	R_1	11 606	Γ_7	11 578
	R_2	11 654	Γ_9	11 690

[a] The associated irreducible representations of D_{3h} group (section 3.2).

centre. Significant differences were noticed between the levels assigned in this paper and those given in table 3 of Verdun *et al* [5]. Within the experimental errors and the shift of the lines with composition, our spectra at low x corresponding to the $^4I_{9/2} \rightarrow {}^4F_{3/2}$ transition are similar to those given in figure 1 of [5]; however, the assignments of $^4F_{3/2}$ and several $^4I_{9/2}$ levels are quite different. The difference is connected to the interpretation of the data in terms of a unique centre in [5]. Strong differences were observed in many other manifolds. The uncontrollable admixture of the spectral data on two different centres makes the energy-level diagram given in [5] of Nd^{3+} in (Nd, Mg) strontium hexa-aluminate unreliable.

3.2. Polarization spectra

In order to obtain information on the local symmetry of a specific centre from polarization data, the measurements in polarized light were focused on the samples with $x = 0.05$ (where the C_2 centre is dominant) and $x = 0.5$ (where the C_1 centre is prevailing). The measurements were performed at 15 and 300 K, in the 11 000–24 000 cm^{-1} spectral range in absorption, with light propagation in the mirror $(\boldsymbol{a}, \boldsymbol{b})$ plane along a crystallographic axis, which is perpendicular

Table 3. Experimental energy levels of the C_2 Nd^{3+} centre in ASN ($x = y = 0.05$) and calculated ones for the D_{3h} local group including the irreducible representations (IR).

	Energy (cm^{-1})				Energy (cm^{-1})		
$^{2S+1}L_J$	Exp.	Theory D_{3h}	IR D_{3h}	$^{2S+1}L_J$	Exp.	Theory D_{3h}	IR D_{3h}
	0	−8	Γ_8		(13 520)	13 538	Γ_8
	110	138	Γ_7	$^4F_{7/2} + {}^4S_{3/2}$	13 567	13 573	Γ_7
$^4I_{9/2}$	155	152	Γ_9		13 714	13 720	Γ_9
	480	482	Γ_9		13 734	13 742	Γ_7
	530	529	Γ_8		13 740	13 750	Γ_9
					(13 803)	13 794	Γ_8
	(2069)	2059	Γ_7				
	2073	2063	Γ_9		14 868	14 872	Γ_7
$^4I_{11/2}$	(2174)	2167	Γ_7		14 893	14 902	Γ_9
	(2208)	2209	Γ_9	$^4F_{9/2}$	(14 940)	14 941	Γ_8
	2235	2236	Γ_8		(14 952)	14 958	Γ_8
	2281	2277	Γ_8		15 015	14 986	Γ_9
	(3990)	3986	Γ_7		16 036	16 033	Γ_7
	(4084)	4085	Γ_7		16 040	16 046	Γ_9
	4105	4105	Γ_9	$^2H_{11/2}$	(16 075)	16 062	Γ_8
$^4I_{13/2}$	(4151)	4153	Γ_7		16 092	16 102	Γ_9
	4185	4187	Γ_8		16 110	16 107	Γ_7
	4266	4266	Γ_9		(16 176)	16 168	Γ_8
	4377	4384	Γ_8				
					17 298	17 305	Γ_9
$^4F_{3/2}$	11 606	11 583	Γ_7		—	17 324	Γ_8
	11 654	11 651	Γ_9		17 342	17 368	Γ_7
				$^4G_{5/2} + {}^2G_{7/2}$	17 465	17 490	Γ_9
	(12 600)	12 610	Γ_8		17 538	17 554	Γ_7
$^4F_{5/2} + {}^2H_{9/2}$	12 639	12 635	Γ_7		(17 557)	17 555	Γ_8
	12 648	12 644	Γ_9		(17 575)	17 578	Γ_8
	12 689	12 668	Γ_9				
	12 703	12 705	Γ_8	$^2P_{1/2}$	23 427	23 422	Γ_7
	12 845	12 861	Γ_7				
	—	12 880	Γ_9				
	(12 972)	12 990	Γ_8				

to *c*. For both crystals, the $\sigma(\vec{E} \perp c)$ lines are more intense than the $\pi(\vec{E} \parallel c)$ ones ($\vec{E}$ is the electric field direction). We shall present details on the polarization data only in several transitions.

The $^4I_{9/2}(Z_1) \rightarrow {}^2P_{1/2}$ absorption lines at 15 K are observed in both σ and π polarizations for both crystals. However, the hot band structure is different for the two crystals, as illustrated in figures 3(a), (b), where part of the 300 K absorption spectra are presented. For $x = 0.05$, a hot band corresponding to the $Z_3 \rightarrow {}^2P_{1/2}$ transition of the C_2 centre (see table 2) in σ polarization is observed in this range, while for the crystal with $x = 0.5$ two hot bands, corresponding to the $Z_2 \rightarrow {}^2P_{1/2}$ and $Z_3 \rightarrow {}^2P_{1/2}$ transitions of the C_1 centre, are present in the σ spectra. For $x = 0.05$ a very weak line corresponding to the $Z_4 \rightarrow {}^2P_{1/2}$ transition shows up in both σ and π spectra, but no other hot bands are observed in the $x = 0.5$ sample, probably due to broadening of the lines.

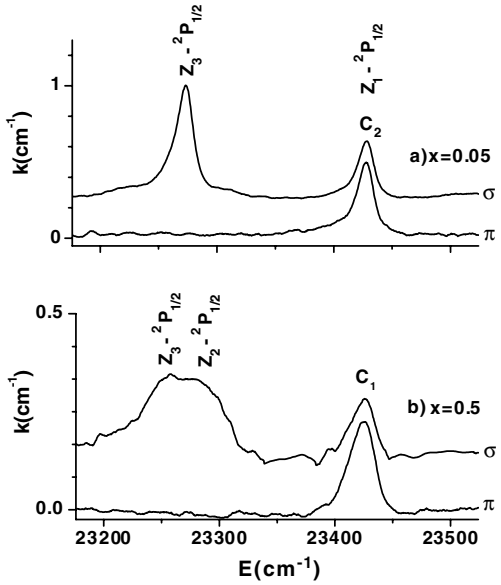

Figure 3. The polarized Nd^{3+} $^4I_{9/2} \rightarrow {}^2P_{1/2}$ absorption spectra at 300 K of two (Ln, Mg) strontium hexa-aluminate samples: (a) $x = y = 0.05$ and (b) $x = 0.5$, $y = 0.05$.

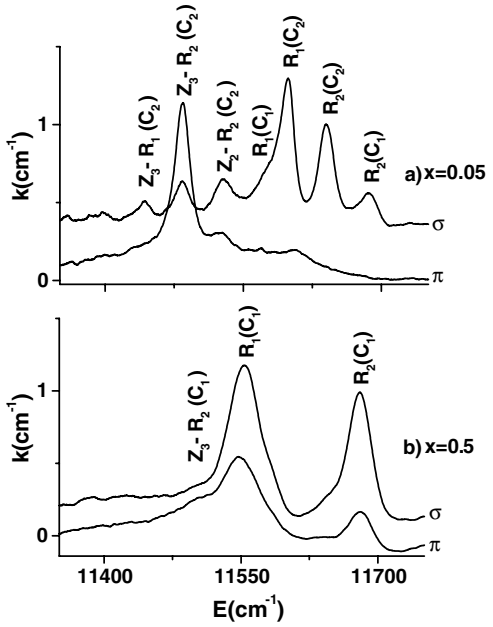

Figure 4. The polarized Nd^{3+} $^4I_{9/2} \rightarrow {}^4F_{3/2}$ absorption spectra at 300 K of two (Ln, Mg) strontium hexa-aluminate samples: (a) $x = y = 0.05$ and (b) $x = 0.5$, $y = 0.05$.

The 300 K $^4I_{9/2} \rightarrow {}^4F_{3/2}$ absorption spectra given in figures 4(a) and (b) also show clear differences between the polarized spectra of the two samples. The polarization effects are very strong for $x = 0.05$, where the most intense lines, assigned as in figure 4(a), belong

Table 4. Electric-dipole selection rules for Kramers ions in D_{3h} symmetry [19], with σ ($\vec{E} \perp c$) and π ($\vec{E} \parallel c$), and $\vec{E}$ being the electric-field direction.

	Γ_7	Γ_8	Γ_9
Γ_7	—	σ, π	σ
Γ_8	σ, π	—	σ
Γ_9	σ	σ	π

to the C_2 centre, while the less intense ones are associated to the C_1 centre. In the case of $x = 0.5$ samples, where the C_1 centres dominates (figure 4(b)), the polarization effects are less pronounced and a single hot band corresponding to $Z_3 \rightarrow R_2$ transition is visible.

In other manifolds clear polarization effects are observed only for the $x = 0.05$ sample. The differences between the polarization spectra for the two centres are analysed in relation to the selection rules for the D_{3h} symmetry group. In a crystal field of D_{3h} symmetry, corresponding to the unperturbed (2d) sites occupied by Nd^{3+}, the J manifolds are split into $(2J + 1)/2$ Stark doublets characterized by the Γ_7, Γ_8 and Γ_9 bi-dimensional irreducible representations. The crystal-field levels of some J manifolds are $D^{1/2} \rightarrow \Gamma_7$, $D^{3/2} \rightarrow \Gamma_7 + \Gamma_9$, $D^{9/2} \rightarrow \Gamma_7 + 2\Gamma_8 + 2\Gamma_9$. The electric-dipole selection rules for D_{3h} point group [18, 19] are given in table 4 with σ ($\vec{E} \perp c$) and π ($\vec{E} \parallel c$) polarization. For lower symmetries the selection rules relax, and for groups with symmetries lower than C_{2v} all the transitions are electric-dipole allowed.

Since the $^4I_{9/2}(Z_1) \rightarrow {}^2P_{1/2}(\Gamma_7)$ absorption line for the C_2 centre ($x = 0.05$) has similar intensity in both polarizations, the ground Stark level Z_1 of $^4I_{9/2}$ could be associated to a Γ_8 representation. This assignment can be verified by EPR measurements, since quite different g-factors are expected if Γ_7 ($g_\perp = 5g_\parallel$), Γ_9 ($g_\perp = 0$) or Γ_8 ($g_\parallel \sim 4$, $g_\perp \sim 2$) is the ground state [20]. The EPR spectra of Nd^{3+} in hexa-aluminates at low x show at $\vec{B} \parallel \boldsymbol{c}$ a single sharp line, while at $\vec{B} \perp \boldsymbol{c}$ there is a nearly isotropic very broad line [3, 4, 21]. In the low-resolution spectra [21] a gradual shift and broadening of the lines as x increases has been observed. The recent EPR data [22, 23] for ASN: Nd ($x = y = 0.01$) reported $g_\parallel = 3.75$ and $g_\perp = 1.76$ and more complex behaviour at higher x. These data sustain Γ_8 as the ground state.

The observed polarization effects in the 15 and 300 K absorption spectra for many transitions of the C_2 centre can be consistently explained with the selection rules of D_{3h} symmetry (table 4), if the symmetry (irreducible representations IR) of the $^4I_{9/2}$ and $^4F_{3/2}$ Stark components are as given in column 4 of table 2. For instance, the $Z_{1,4}(\Gamma_8) \rightarrow {}^2P_{1/2}$ (Γ_7) lines are observed in both polarizations, $Z_2(\Gamma_7) \rightarrow {}^2P_{1/2}$ (Γ_7) is strictly forbidden and $Z_{3,5}(\Gamma_9) \rightarrow {}^2P_{1/2}$ (Γ_7) are seen only in σ spectra. Similarly, for $^4I_{9/2} \rightarrow {}^4F_{3/2}$ absorption (figure 4(a)): $Z_1(\Gamma_8) \rightarrow R_1(\Gamma_7)$ is observed in both polarizations, $Z_3(\Gamma_7) \rightarrow R_1(\Gamma_7)$ is strictly forbidden, $Z_1(\Gamma_8) \rightarrow R_2(\Gamma_9)$, $Z_2(\Gamma_7) \rightarrow R_2(\Gamma_9)$ and $Z_3(\Gamma_9) \rightarrow R_1(\Gamma_7)$ are observed only in σ spectra and $Z_3(\Gamma_9) \rightarrow R_2(\Gamma_9)$ in π spectra. IRs were associated to many other Stark levels.

The interpretation of the polarization data for the C_1 centre in the $x = 0.5$ sample is more difficult, and indicates an obvious lowering in symmetry from the ideal D_{3h}. Thus, in the $^4I_{9/2} \rightarrow {}^2P_{1/2}$ range (figure 3(b)) the σ spectrum contains a hot band corresponding in D_{3h} to a $Z_2(\Gamma_7) \rightarrow {}^2P_{1/2}(\Gamma_7)$ transition, forbidden in D_{3h}, and not present for C_2 centres. For the $^4I_{9/2} \rightarrow {}^4F_{3/2}$ transition (figure 4(b)) the $Z_1(\Gamma_8) \rightarrow R_2(\Gamma_9)$ line is detected in both σ and π spectra and a weak hot band $Z_3(\Gamma_9) \rightarrow R_2(\Gamma_9)$, forbidden in σ polarization in D_{3h}, is also observed. These data indicate an obvious lowering in symmetry from the ideal D_{3h} symmetry of the (2d) sites for C_1 centres.

3.3. The models for non-equivalent Nd^{3+} centres in ASN and ASL

The new spectroscopic data obtained in this work enable the refinement of the structural models [15] for the non-equivalent Nd^{3+} centres in magnesium-compensated strontium hexaaluminates $Sr_{1-x}Nd_yLa_{x-y}Mg_xAl_{12-x}O_{19}$.

The barycentres of the manifolds are mainly determined by the nature and structure of the first anionic coordination sphere, via the nephelauxetic effect [11, 12, 24]. Thus, the closeness of the energies of the barycentres of the C_1 and C_2 centres and their quite high energy indicate that the Nd^{3+} ions occupy, for both classes of centre, large (2d) sites with the same ionic coordination to 12 O^{2-}. At the same time, the strong differences between the crystal-field effects in the $^4F_{3/2}$ manifold for these centres (table 1) and less in other manifolds, suggest that the changes are induced by more distant perturbations that influence mainly the second-order parameters B_q^2 and less the fourth- or sixth-order ones. Such perturbations can originate from the cationic disorder of the nearest coordination spheres around the Nd^{3+} ion. In ASL, Sr^{2+} and Ln^{3+} (Nd^{3+} or La^{3+}) can occupy large (2d) sites and Mg^{2+} enter in Al^{3+} sites. The main effects in the crystal field at the Nd^{3+} ion are expected from the electric charge differences. The spectral effects of this disorder are further analysed.

The probability of occurrence of the structural centres. The experimental composition dependence of the relative intensity of the C_1 centre to the total intensity of the spectra ($C_1 + C_2' + C_2''$) satisfies the $1-(1-x)^6$ law for the entire composition range (figure 1(b)). This dependence corresponds to the calculated probability of random and equiprobable occupation of the nearest-neighbour (2d) coordination sphere (at 5.56 Å) by one to six trivalent Ln^{3+} (Nd^{3+} or La^{3+}) ions replacing bivalent Sr^{2+} ions and the assumption that the integral absorption cross-sections for the two centres are almost equal. The probability of occurrence of a perturbed centre with n out of the m available sites on a given coordination sphere around the central Nd^{3+} ion is

$$P_{mn} = \frac{m!}{(m-n)!n!} p^n (1-p)^{m-n} \tag{1}$$

where p is the probability of occupation of a site on this sphere. For random equiprobable placement of Ln^{3+} in the (2d) sites, $p = x$. The probability of occurrence of the centres with *no* Ln^{3+} ions on the first coordination sphere of six (2d) sites—C_2 centres—is $(1-x)^6$, while the global probability of occurrence for all the perturbed centres having *one to six* Ln^{3+} ions on this sphere would be equal to $1-(1-x)^6$–C_1 centres. The data for $x = 0.5$ confirm the saturation character of the dependence on x for C_1 centres. The assumption that the integral absorption cross-sections for the two centres are similar is based on the fact that for the transitions between ^4I_J and $^4F_{3/2}$ manifolds, the Ω_2 Judd–Ofelt parameter, which contains the low-k crystal-field terms that are more influenced by the distant cationic perturbations, is zero. On the other hand, the high-k crystal-field terms, which influence the active Judd–Ofelt parameters of these transitions, are less sensitive to distant perturbations.

This structural model for the C_1 and C_2 families of centres is consistent with the emission decay measurements on ASL: Nd crystals [15] with $x = 0.2$–0.4 and $y = 0.05$–0.15: the emission decay for the two centres differs only at early times up to $\sim$200 μs, being faster for C_1; then they run in parallel. It was inferred that this difference originates from the energy transfer inside the first Nd^{3+}–Nd^{3+} pairs that, according to this structural model, are possible only for C_1 centres. The effect of the energy transfer on the emission decay of the C_2 centre where the nearest-neighbour Nd^{3+} pairs are excluded indicates that this transfer is induced mainly by electric-dipole interactions between the excited and non-excited Nd^{3+} ions.

The selective perturbing effects of Nd^{3+} and La^{3+} ions. Up to now only the global effect of perturbation due to the electric charge differences between Sr^{2+} and Ln^{3+} ions was considered. The differences between C_1 (La) and C_1 (Nd) lines show that the perturbation is due to both *electric charge and ionic size* differences. Due to the different occupation numbers (1 to 6) and to various possibilities of occupation of nearest sites by Ln^{3+} ions, the C_1 centre corresponds to a family of perturbed structural centres of various local symmetries. This is sustained by the shapes and widths of the lines. The perturbations produced by Ln^{3+} in sites from other (2d) coordination spheres are not resolved, owing to the large distances (at minimum 9.62 Å), but they contribute to broadening of C_1 centre lines.

The perturbing effects of Mg^{2+} ions. The spectral effects due to the Mg^{2+} charge-compensator ions are not evident in samples with large x parameters. However, the spectral structure observed for low-x (<0.1) samples in the range of C_2 centre lines, C_2' and C_2'' lines, could be associated to Mg^{2+} effects. As shown in earlier studies [6, 7], the Mg^{2+} ions in ASL substitute preferentially the tetrahedral Al^{3+} sites (Al^{3+}_{tetr}). The closest coordination sphere of Al^{3+}_{tetr} sites at 5.85 Å contains six sites forming two triangles, above and below the mirror plane (figures 5, 6) and do not share common O^{2-} with the central Nd^{3+} ion. However, there are many Al^{3+} sites closer to a (2d) site with other O^{2-} coordinations: 3 bipyramidal at ∼3.2 Å and 24 octahedral sites (at 3.46, 3.47, or 5.26 Å). The crystal-field perturbation due to the charge disorder induced by Mg^{2+} in Al^{3+}_{tetr} sites is weaker than in the case of Ln^{3+} ions due mainly to the much smaller relative concentration of Mg^{2+} to that of all Al^{3+} ions. This is consistent with the small shift between the C_2' and C_2'' centres lines. It is thus very likely that the two components of the C_2 lines reflect the crystal-field perturbing effect of the Mg^{2+} ions: the C_2'' centre could correspond to a Nd^{3+} centre *without any Mg^{2+} ion* in the nearest coordination sphere of Al^{3+}_{tetr} sites, while the component C_2' corresponds to Nd^{3+} ions with such perturbing Mg^{2+} ions on this sphere. The C_2 centres, having no Ln^{3+} near neighbours, require only the charge compensation of the central Nd^{3+} ion. The statistics of distribution of the Mg^{2+} ions is complex, since the placement of the Mg^{2+} ions would not be random and independent of the placement of the Ln^{3+} ions, but it will be rather *correlated* with it, i.e., the Mg^{2+} ions will have the tendency to replace Al^{3+} ions in vicinity of the Ln^{3+} ions. Obviously, the Mg^{2+} ions perturb the crystal field of the C_1 centres too: in this case more than one Mg^{2+} ion could be present on the near-neighbour tetrahedral coordination sphere, in correlation with the occupation of the nearest (2d) coordination sphere by Ln^{3+} ions.

The polarization effects and local symmetry of the centres. The polarization data show that the local symmetry for the C_2 centres is very close to D_{3h}, while it is lower for C_1 centres. Since the central Nd^{3+} ion shares the surrounding O^{2-} ions with the near-neighbour (2d) sites, the presence of Ln^{3+} ions in these sites could distort by electric charge or ionic size the anionic environment, leading to lowering of the local symmetry for C_1 centres. These facts sustain the results of x ray measurements [4] for high x parameter.

Another argument for a unique centre model has been based on the EPR data [3, 4, 21]. The low-resolution EPR spectra of Nd^{3+} in hexa-aluminates show at $\vec{B} \parallel \boldsymbol{c}$ a single sharp line, while at $\vec{B} \perp \boldsymbol{c}$ they show a nearly isotropic very broad one [3, 4] and a gradual shift and broadening of the lines as x increases [21]. Recent EPR measurements [22, 23] at 15 K on $Sr_{1-x}Nd_xMg_xAl_{12-x}O_{19}$ (ASN) crystals with $x \leqslant 0.2$ show that, if at low x the spectrum with the magnetic field parallel to the $\boldsymbol{c}$-axis contains a single line, at larger Nd^{3+} concentrations, several pairs of satellites placed almost symmetrically around this line were observed. At higher x or in lanthanum hexa-aluminates [21] this structure is not resolved in the EPR spectra.

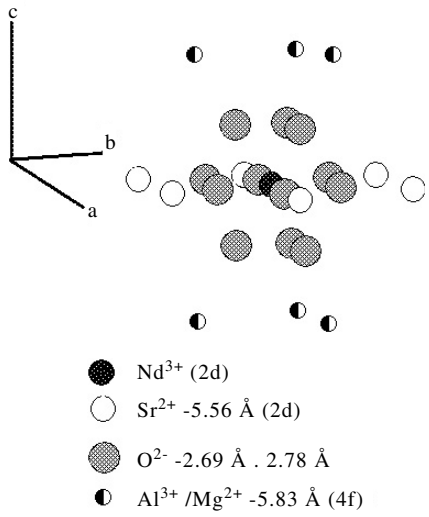

Figure 5. The structural model for C_2 Nd^{3+} centres in (Ln, Mg) strontium hexa-aluminates; only the important near neighbours are presented: 12 oxygens, six Sr^{2+} in nearby (2d) sites and no Mg^{2+} in nearby Al^{3+}_{tetr} sites for C_2'' and up to one Mg^{2+} in these sites for C_2' are represented.

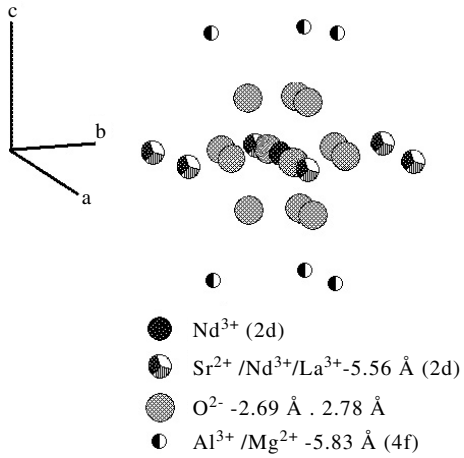

Figure 6. The structural model for C_1Nd^{3+} centres in (Ln, Mg) strontium hexa-aluminates; only the important near neighbours are presented: 12 oxygens, the six Sr^{2+} in the nearby (2d) sites are replaced by one to six Ln^{3+} and more than one Mg^{2+} ions are in the nearby Al^{3+}_{tetr} sites.

The group of most intense four satellites has been assigned [22, 23] to a well-definite type of pairs of Nd^{3+} ions with the pair axis perpendicular to $\boldsymbol{c}$, although the strong inhomogeneous broadening of EPR lines for $\vec{B} \perp \boldsymbol{c}$ reflects the presence of a variety of structural centres. In order to account for the four-line structure, it was considered that the two Nd^{3+} centres from the pair have slightly different structures that determine a small difference in the $g_{\|}$ factors, without a definite structure of these centres.

It is very likely that the single-line EPR centre reported at small x corresponds to the C_2 centre (C_2' and C_2'') that, in our model, has no Nd^{3+} near neighbour to form a pair; its relative intensity with respect to the whole EPR spectrum is expected to decrease as x increases, as

experimentally observed [22, 23]. The C_1 centres in ASN are in fact pairs or higher assemblies of Nd^{3+} ions in the nearest-neighbour (2d) sites and there is a quite large variety of such pairs. EPR pairs could correspond to C_1 centres for which the surrounding of the Nd^{3+} ions differs, for instance by the composition of the nearest Al^{3+}_{tetr} sphere. The gradual shift of the g-values and the broadening of EPR lines with x could indicate the increasing complexity of C_1 centres connected with the structural disorder in the (2d) and Al^{3+}_{tetr} sites.

3.4. Crystal-field analysis

Based on the experimental energy levels for the Nd^{3+} $C_2 \equiv C_2'$ centre (table 3) in the $x = y = 0.05$ sample, a crystal-field calculation was performed considering the D_{3h} local symmetry. The crystal-field potential for D_{3h}, $V_{D_{3h}} = \sum_{k,q} B_q^k V_q^k$, contains only four terms, with ($k = 2, 4, 6$, $q = 0$) and ($k = 6$, $q = 6$). The free-ion parameters taken from Alablanche *et al* [4] and crystal-field parameters for the D_{3h} group were refined by using the IMAGE program [25]. The best-fit crystal-field parameters (in cm^{-1}) are $B_0^2 = 516.6$, $B_0^4 = 464.8$, $B_0^6 = -1611$ and $B_6^6 = 1145$ and the calculated Stark levels with a mean deviation of 10.5 cm^{-1} for 65 levels and the irreducible representations (IR) labels are given in table 3. The experimentally assigned symmetry characteristics from polarization spectra were used as an additional check. The position of the levels, taking into account the uncertainty of some assignments, and their symmetry characteristics are rather well described by these parameters. Significant discrepancies with the previously reported crystal-field parameters [5] are essentially due to assignment of the experimental levels, based in our case on the two-centre model.

The strong dependence on the composition of the C_1 centre spectra and the lack of a definite symmetry for this centre makes a crystal-field analysis unreliable.

3.5. Connection with laser properties

The selectively excited luminescence spectra in all ranges of interest for laser emission (0.9 $\mu m\, {}^4F_{3/2} \rightarrow {}^4I_{9/2}$, 1.0 $\mu m\, {}^4F_{3/2} \rightarrow {}^4I_{11/2}$ and 1.3 $\mu m\, {}^4F_{3/2} \rightarrow {}^4I_{13/2}$ ranges) are different for the C_1 and C_2 Nd^{3+} centres (figure 2). The absorption spectroscopy evidences two absorption regions, (${}^4I_{9/2} \rightarrow {}^4F_{5/2}$) and (${}^4I_{9/2} \rightarrow {}^4F_{3/2}$), favourable for diode laser longitudinally pumping of crystals cut perpendicular to the $\boldsymbol{c}$-axis. The room-temperature ${}^4I_{9/2} \rightarrow {}^4F_{5/2}$ absorption presents two intense bands at 798 nm (hot band) and 791 nm, of similar intensities, but with partial superposition the centre bands of C_1 and C_2. This could induce lasing at two different wavelengths, instabilities or uncontrollable jumping of emission wavelength; thus, the use of crystals with dominance of one of these centres would be recommended.

In the case of direct pumping in the metastable level, the ${}^4I_{9/2} \rightarrow {}^4F_{3/2}$ absorption spectra of the two centres are better separated and almost selective pumping can be achieved. The integral absorption cross-section for the two centres are almost equal. The larger linewidth makes the peak absorption cross-sections for the C_1 centre smaller than for C_2. The partial superposition of the $Z_1 \rightarrow R_1$ and $Z_3 \rightarrow R_2$ transitions lines of the C_1 centre around 865 nm contributes to an increased integrated absorption. Thus, while narrow-band pumping, such as with a Ti:sapphire laser, of the C_2 centre in the ${}^4I_{9/2} \rightarrow {}^4F_{3/2}$ lines could be favourable due to the larger peak absorption, diode laser pumping in both the ${}^4I_{9/2} \rightarrow {}^4F_{5/2}$ and ${}^4I_{9/2} \rightarrow {}^4F_{3/2}$ absorption ranges of the C_1 centre will be more efficient. The composition dependence of the probability of occurrence of these centres and the crystal growth conditions indicate as a favourable choice the compositions with parameter $x \geqslant 0.4$, where the C_1 centres are over

95% abundant. These conclusions are consistent with the recent 901 nm laser studies on Nd: ASL crystals with $x = 0.4$ that show [17] a higher laser efficiency (slope efficiency 0.74) with pumping at 791 nm than the crystals with $x = 0.3$ used earlier (slope efficiency 0.58), while the direct 865 nm pumping in $^4F_{3/2}$ produced laser emission with slope efficiency [26] of 0.84, much higher than for any other quasi-three-level Nd^{3+} laser emission reported so far.

4. Conclusion

An analysis of the non-equivalent Nd^{3+} centres in disordered ASL: Nd—$Sr_{1-x}Nd_yLa_{x-y}Mg_xAl_{12-x}O_{19}$ crystals, based on new high-resolution optical spectroscopy data (including polarization) on an extended composition range ($0.01 \leqslant x \leqslant 0.5$), was performed. The previous division [15] in two main classes of Nd^{3+} centre, C_1 and C_2, is preserved. A doublet structure was resolved in C_2 lines (C_2' and C_2'' components) at low x and the effects that could be assigned to the ionic size difference between Nd^{3+} and La^{3+} ions were also noticed in the C_1 centre spectral range. It was concluded that whereas for C_2 (C_2' and C_2'') centres the nearest-neighbour (2d) coordination sphere is occupied only by Sr^{2+} ions, in the case of C_1 centres one up to all the six sites of this sphere are occupied by Ln^{3+} (Nd^{3+} or La^{3+}) ions. The difference between the C_2' and C_2'' centres is tentatively connected by the perturbing effects of the Mg^{2+} ions at the nearest tetrahedral Al^{3+} sites: with no Mg^{2+} for C_2'', and one Mg^{2+} for C_2'. It is inferred that the distribution of trivalent Ln^{3+} ion at the (2d) sites is random, while that of Mg^{2+} is rather correlated with the distribution of the Ln^{2+} ions. The polarization data that suggest a D_{3h} symmetry for C_2 and lower for the C_1 centre and the emission decay data are consistent with these models.

A comparative examination of the previous published optical spectroscopic data (energy-level scheme, polarization effects, crystal-field parameters, etc) of Nd^{3+} in strontium hexa-aluminates, interpreted in terms of a unique centre model or EPR data shows definitely that such a model cannot consistently describe any of these data. The results of this study can be extended to the investigation of other laser ions or to the luminescent phosphors based on Sr^{2+} or Ca^{2+} hexa-aluminates.

References

[1] Wickoff R W G 1965 *Crystal Structure* vol 3 *Inorganic Compounds* (New York: Interscience)
[2] Bagdasarov Kh S, Kaminskii A A, Kevorkov L, Li, Prokhorov A M, Sarkisov S E and Tevosyan T A 1974 *Sov. Phys.—Dokl.* **19** 350
[3] Alablanche S, Collongues R, Leduc M, Minvielle A, Thery J and Vivien D 1991 *J. Physique Coll.* IV **1** C7 275
[4] Alablanche S, Kahn-Harari A, Thery J, Viana B, Vivien D, Dexpert-Ghys J and Faucher M 1992 *J. Solid State Chem.* **98** 10
[5] Verdun H R, Wortman D E, Morrison C A and Bradshaw J L 1997 *Opt. Mater.* **7** 117
[6] Kahn A, Gasperin M, Saine M C, Lejus A M, Thery J and Vivien D 1988 *J. Chem. Phys.* **88** 8018
[7] Xie L and Cormack A N 1989 *J. Solid State Chem.* **83** 282
[8] Delacarte V, Thery J and Vivien D 1994 *J. Physique Coll.* IV C4 **4** 361
[9] Delacarte V, Thery J and Vivien D 1994 *J. Lumin.* **62** 237
[10] Delacarte V, Thery J, Benitez J M, Vivien D, Borel C, Templier R and Wyon C 1995 *OSA Proc. Adv. Solid State Lasers* **24** 123
[11] Kettle S F A 1996 *Physical Inorganic Chemistry, A Coordination Chemistry Approach* (Oxford: Spectrum Academic Publishers)
[12] Vivien D 2004 *Proc. SPIE* **5581** 56
[13] Aka G, Reino E, Vivien D, Balembois F, Georges P and Ferrand B 2002 *Trends Opt. Photon.* **68** 329
[14] Vivien D, Aka G, Lupei A, Lupei V and Gheorghe C 2004 *Proc. SPIE* **5581** 287
[15] Lupei A, Lupei V, Gheorghe C, Vivien D, Aka G and Aschehoug P 2004 *J. Appl. Phys.* **96** 3057
[16] Lupei A, Lupei V, Gheorghe C, Gheorghe L, Vivien D and Aka G 2005 *Phys. Status Solidi* c **2** 276

[17] Aka G, Vivien D and Lupei V 2004 *Appl. Phys. Lett.* **85** 2685
[18] Koster G F, Dimmock J O, Wheeler R G and Statz H 1963 *Properties of the Thirty-two Point Groups* (Cambridge, MA: MIT Press)
[19] Hufner S 1978 *Optical Spectra of Transparent Rare earth Compounds* (New York: Academic)
[20] Abragam A and Bleaney B 1970 *Electron Paramagnetic Resonance of Transition Ions* (Oxford: Clarendon)
[21] Gbehi T, Thery J, Vivien D, Collongues R, Dhalenne R and Revcolevschi A 1988 *J. Solid State Chem.* **77** 211
[22] Guillot-Noel O, Goldner Ph, Higel P and Gourier D 2003 *Chem. Phys. Lett.* **380** 563
[23] Guillot-Noel O, Goldner Ph, Higel P and Gourier D 2004 *J. Phys.: Condens. Matter* **16** (3) R1
[24] Antic-Fidancev E 2000 *J. Alloys Compounds* **300/301** 2
[25] Porcher P, Computer code IMAGE, unpublished
[26] Lupei V, Aka G and Vivien D 2005 *Trends Opt. Photon.* **98** 177